

1
2
3
4
5
6
7
8
9
10
11
12
13
14
15
16
17
18
19
20
21
22
23
24
25
26
27
28
29
30
31
32
33
34
35
36
37
38
39
40
41
42
43
44
45
46
47
48
49
50
51
52
53
54
55
56
57
58
59
60
61
62
63
64
65

Comparison of crystallization characteristics and mechanical properties of polypropylene processed by ultrasound and conventional micro injection molding

Davide Masato^{a,b,†}, Maksims Babenko^a, Banah Shriky^a, Tim Gough^a, Giovanni Lucchetta^b, Ben
Whiteside^a

^a Faculty of Engineering and Informatics, University of Bradford, Bradford, UK

^b Department of Industrial Engineering, University of Padova, via Venezia 1, Padova, Italy

[†] corresponding author, davide.masato@phd.unipd.it

1
2
3
4 **Comparison of crystallization characteristics and mechanical properties of polypropylene**
5
6 **processed by ultrasound and conventional micro injection molding**
7
8

9 Davide Masato, Maksims Babenko, Banah Shriky, Tim Gough, Giovanni Lucchetta, Ben Whiteside
10
11

12
13
14 **Abstract.** Ultrasound injection molding has emerged as an alternative production route for the
15
16 manufacturing of micro scale polymeric components, where it offers significant benefits over the
17
18 conventional micro injection molding process. In this work, the effects of ultrasound melting on the
19
20 mechanical and morphological properties of micro polypropylene parts were characterized. The
21
22 ultrasound injection molding process was experimentally compared to the conventional micro injection
23
24 molding process using a novel mold, which allows mounting on both machines and visualization of the
25
26 melt flow for both molding processes. Direct measurements of the flow front speed and temperature
27
28 distributions were performed using both conventional and thermal high-speed imaging techniques. The
29
30 manufacturing of micro tensile specimens allowed the comparison of the mechanical properties of the
31
32 parts obtained with the different processes. The results indicated that the ultrasound injection molding
33
34 process could be an efficient alternative to the conventional process.
35
36
37
38
39
40
41
42

43 **Keywords:** ultrasound injection molding; micro injection molding; mechanical properties;
44
45 morphology; flow visualization
46
47
48
49
50
51
52
53
54
55
56
57
58
59
60
61
62
63
64
65

1. Introduction

In microsystems technology, polymer micro components have been attracting large attention for several applications, such as micro electronics, micro mechanics, micro optics and micro biomedical devices [1-5]. However, the increasing market trend needs to be sustained by the development of effective manufacturing processes that could support their mass production [6,7].

Micro injection molding (μ IM) is one of the most popular manufacturing technologies used to produce thermoplastic micro components, which typically have sub-100 mg masses and dimensions or tolerances in the micrometer range [8,9]. The process depends fundamentally on the molten polymer accurately replicating the mold geometry during the mold filling and cooling phases through a complex mechanism [10], which is determined by the complicated relationship between materials properties, processing conditions and mold geometry [11-13].

Despite the significant improvements and the ongoing research, the quality of μ IM parts is still hindered by some intrinsic process limitations. Lucchetta et al. investigated the technological limits of μ IM observing that the achievement of optimum quality of the molded parts is still challenging, even using state-of-the-art μ IM process technology (i.e. rapid heat cycle molding and cavity air evacuation) [14]. Indeed, the uneven distribution of cavity pressure hindered the achievement of a complete and homogenous replication of a high aspect ratio micro-structured surface. In fact, the filling phase of the μ IM process is characterized by highly shear-stressed melt along the flow direction, which leads to anisotropy in the properties of the final molded parts [15].

Moreover, the μ IM process is significantly affected by complex boundary conditions due to the marked thermal gradients and the typically very small cavity thicknesses [16]. These conditions affect the formation of the 'skin-core' morphology and are the cause for the nucleation and the formation of smaller and more oriented crystalline structures within the molded parts [17].

1
2
3
4 In this context, some new process concepts have emerged aiming at improving processing
5
6 performances and the quality of the molded micro parts. In particular, ultrasound injection molding
7
8 (usIM) was proposed due to the interesting benefits it could yield compared to the conventional μ IM
9
10 process [18].
11

12
13
14 The usIM process is characterized by the use an ultrasound horn for the melting of the polymer
15
16 pellets [19]. The energetic ultrasound waves are exploited to cyclically heat and deform the polymer at
17
18 ultrasound frequencies. The melting of the polymer is then controlled by the friction heating at the contact
19
20 points between the pellets and by the viscoelastic heating generated by the damping of the ultrasonic
21
22 oscillation within the polymer itself [20,21].
23
24

25
26 A conventional injection molding plastication unit typically comprises of a reciprocating screw and
27
28 a barrel with electrical heaters. The energy required to heat a volume of material for a single shot is
29
30 relatively high due to heat losses to the environment and the heating of materials that will not contribute
31
32 to the manufactured components (including waste materials generated during purging and the heat
33
34 required to bring the barrel and screw to the set melt temperature) [18]. In ultrasound injection molding,
35
36 significantly lower energy is required for the melting of the polymer due to the absence of electrical
37
38 heaters and no requirement to pre-heat the components of the machine. Moreover, with ultrasound
39
40 melting there is no material residence time and consequent degradation, which is particularly important
41
42 for temperature sensitive polymers. In addition, the ultrasound melting energy is provided only to the
43
44 pellets that are in contact with the sonotrode, thus for each molding cycle only the material required for
45
46 the single shot is melted [19].
47
48
49
50
51

52
53 Other advantages of the usIM process include the reduction of material wastage, which is
54
55 particularly important for micro molding applications where the size of the parts can be significantly
56
57 smaller than the runners and the polymers can be very expensive (e.g. biomedical applications).
58
59
60
61
62
63
64
65

1
2
3
4 Moreover, no purging is required for material changes and cleaning, hence reducing the risk for cross
5
6 contamination.
7

8
9 The ultrasonic energy can also be sustained during the injection phase in order to continuously
10 provide heat to the polymer during cavity filling and consequently reduce the required injection pressure
11 [22]. Moreover, the sprue acts as an ‘energy director’ that is able to orientate the ultrasonic waves in the
12 flow direction. The enhanced flowability of the melt polymer can then be exploited to achieve higher
13 molecular chain relaxation and reduced residual stresses in comparison with conventional μ IM [23,24].
14
15
16
17
18
19
20

21 Despite the significant advantages, the usIM has been poorly investigated in the literature and it is
22 still difficult to control. Sacristán et al. investigated the effects of the ultrasonic vibration on the
23 manufacturing of different parts using polylactide [25]. They have reported that the process requires
24 optimization in order to control material degradation and to avoid incomplete filling of the cavity.
25 Grabalosa et al. successfully manufactured some dumbbell shaped polyamide tensile specimens
26 observing that the combination of vibration amplitude, applied pressure and vibration time determines
27 the amount of ultrasonic energy that is transferred to the polymer pellets [26]. Moreover, they reported
28 that the effect of processing parameters is still unknown and the optimization is complex as it can affect
29 parts filling, morphology and mechanical properties.
30
31
32
33
34
35
36
37
38
39
40
41

42
43 The main process parameters are the amplitude of the vibration, the sonicating time and the applied
44 force. Thus, compared to μ IM, process control for usIM can be significantly different, indicating the
45 necessity of improving the understanding of the process [27]. In this sense, Negre et al. investigated the
46 effects of some process parameters, showing how to approach process optimization (e.g. increased
47 ultrasound time and low injection speed improve the filling) and reporting significant variability in filling
48 length and parts weight [28].
49
50
51
52
53
54
55
56

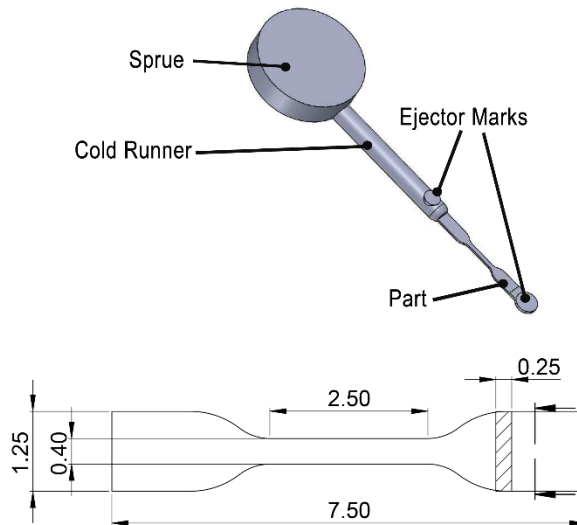
57 In this work, the effect of ultrasound injection molding on the mechanical properties of
58 polypropylene micro parts produced was investigated. A novel injection molding tool, which allows the
59
60
61
62
63
64
65

1
2
3
4 visualization of the melt flow through a sapphire window, was used to produce micro tensile samples
5
6 using both conventional and ultrasound injection molding. The processes were analyzed and compared
7
8 using both conventional and infrared high-speed imaging in order to relate their filling behavior and
9
10 temperature distribution to parts mechanical and morphological properties.
11
12
13
14
15

16 2. Materials and methods

17 2.1 Part design

18
19 The part considered in this study is a micro tensile bar, which dimensions were designed according
20
21 to ISO 527-1 Type 5A and scaled-down by a factor of ten (Fig. 1). In the mold, the cavity was placed on
22
23 the moving half, at the end of semi-cylindrical cold runner (diameter: 2 mm, length: 16 mm long).
24
25
26
27
28
29
30
31



50
51 Figure 1. Design of the molded micro part. All dimensions are in millimeters.
52
53
54

55 A commercial crystalline polypropylene-homopolymer (INEOS PP GA12) was selected for the
56
57 molding experiments. The polymer is characterized by high flowability, high transparency, good
58
59
60
61
62
63
64
65

1
2
3
4 dimensional stability and melt flow rate (MFR) consistency, which makes it ideal for micro molding
5
6 applications. Table 1 reports the main properties of the selected polymer.
7
8
9

10
11 Table 1. Main properties of the polymer selected for the molding experiments.
12
13

Property	Units	Test Method	Value
Density	g/cm ³	ISO 1183	0.93
MFR (230°C – 2.16 kg)	g/10min	ISO 1133	12
Transition Temperature	°C	ISO 6721	182

2.2 Ultrasound injection molding

23
24
25
26 An ultrasound vertical molding machine (Sonus 1G, Ultrason S.L.) was used for the ultrasound
27
28 injection molding (usIM) experiments. The machine is characterized by an ultrasound horn that is used
29
30 to melt the polymer by exploiting the energy transmitted to the polymer through the ultrasonic vibrations.
31
32 A digital ultrasound generator (Branson, 50DCXs30VRT) controls the amplitude and the duration of the
33
34 vibration, with a frequency of 30 kHz and a maximum power of 1.5 kW. The piezoelectric transducer is
35
36 used to convert high-frequency electrical signals into a mechanical vibrations.
37
38

39
40 For each molding cycle, a predefined number of standard polymer pellets is counted by a laser
41
42 system and dosed into the metering chamber (Fig. 2 (a)). Then, the sonotrode, which is fitted on the upper
43
44 mold half, moves down to the injection position (Fig. 2 (b)). The injection is carried out by a vertical
45
46 plunger (8 mm diameter) fitted in the lower half of the mold, which moves upwards pushing the polymer
47
48 pellets towards the vibrating ultrasound horn. The mechanical vibration melts the polymer granules that
49
50 are simultaneously injected into the cavity (Fig. 2 (c)). The ultrasonic vibration was sustained for the
51
52 whole duration of the injection phase.
53
54
55
56
57
58
59
60
61
62
63
64
65

1
2
3
4
5
6
7
8
9
10
11
12
13
14
15
16
17
18
19
20
21
22
23
24
25
26
27
28
29
30
31
32
33
34
35
36
37
38
39
40
41
42
43
44
45
46
47
48
49
50
51
52
53
54
55
56
57
58
59
60
61
62
63
64
65

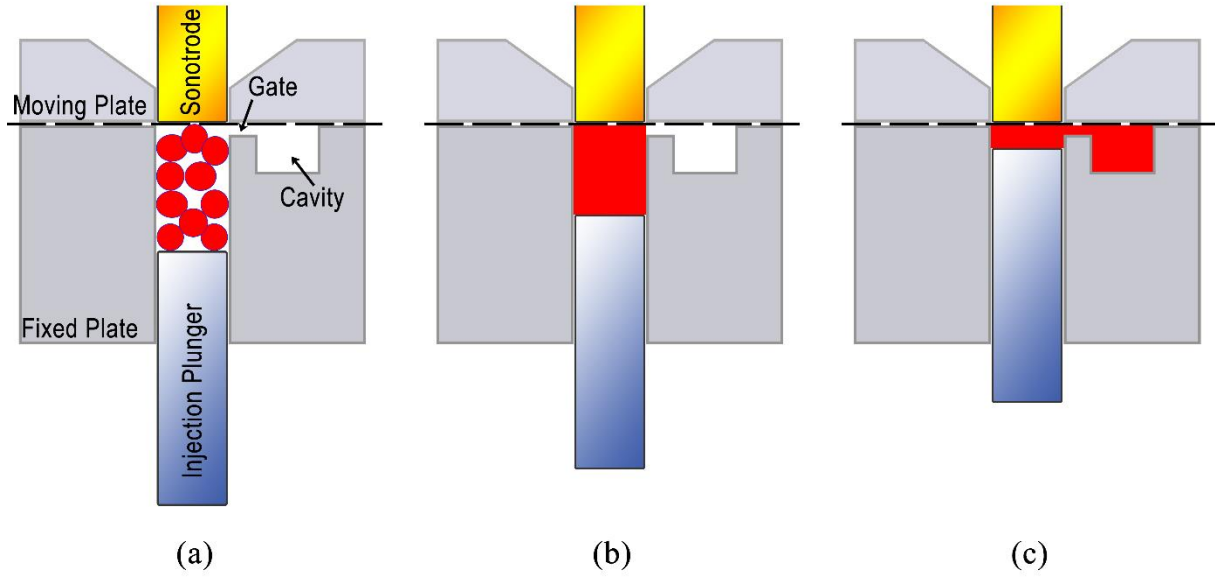


Figure 2. Main phases of the usIM process, (a) pellet feeding and compression, (b) melting, (c) injection.

2.3 Micro injection molding

A state-of-the-art Wittmann Battenfeld, MicroPower 15 electric machine was used for the micro injection molding (μ IM) experiments. The machine is characterized by the separation of the metering and injection systems: the polymer pellets are melted by the mechanical action of a 14 mm plasticizing screw and electrical heaters, while injection is performed by a separated 5 mm injection plunger. The maximum injection speed is of 750 mm/s, to achieve a maximum injection pressure of 2700 bar and a maximum shot size of 1 cm³.

2.4 Mold design

The mold assembly was designed, from a Hasco K-standard modular system, to be mounted on both the usIM and μ IM machines. Minor modifications were only introduced to allow coupling with the different injection units.

1
2
3
4
5
6
7
8
9
10
11
12
13
14
15
16
17
18
19
20
21
22
23
24
25
26
27
28
29
30
31
32
33
34
35
36
37
38
39
40
41
42
43
44
45
46
47
48
49
50
51
52
53
54
55
56
57
58
59
60
61
62
63
64
65

The mold was designed to allow the direct visualization of the polymer melt flow during molding cycles on both machines [29]. A sapphire window (diameter: 26.5 mm, thickness: 4 mm) was placed on the fixed mold half, as shown in Fig. 3. A rectangular pocket was machined on the clamping plate in order to fit a 45° tilted first surface gold mirror, which was mounted and aligned with the center of the cavity.

The mold temperature was set using four electrical cartridge heaters, placed in couples in the mold fixed and moving halves together with a thermocouple.

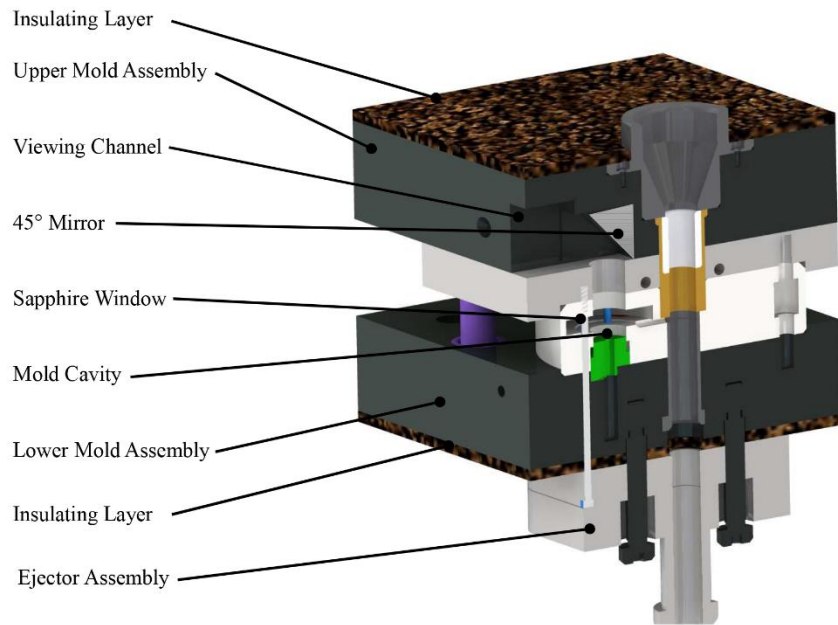


Figure 3. Mold design, as mounted on the usIM machine, and indication of its main components.

2.5 Experimental approach

The analysis of the effects of ultrasound melting on the mechanical properties of micro-molded polypropylene parts was approached by direct comparison with conventional μ IM. The main process

1
2
3
4 parameters were set the same in the two experimental setups, considering the literature, recommendations
5
6 of the material supplier and technological limitations of the machines:
7

- 8 • mold temperature: 80 °C;
- 9
- 10 • cooling time: 5 s;
- 11
- 12 • clamping force: 150 kN
- 13
- 14 • set flow rates: 2,500; 5,000; 10,000 mm³/s.
- 15
- 16
- 17
- 18

19 In the usIM machine, for each cycle seven pellets were dosed into the metering chamber (8 mm
20 diameter, 6 mm length) before the beginning of the injection, which was performed with an applied force
21 of 700 N. The ultrasound vibration was controlled by setting an amplitude of 0.9 of the maximum (i.e.
22 10 μm) and a sonicating time of 3 seconds.
23

24 For the μIM process, the melt temperature was set to 220 °C and the shot size was fixed to the value
25 of 1.2 mm. The switch-over point was set at the 80% of the injection pressure peak, while a packing
26 pressure of 500 bar for 3 seconds was applied.
27

28 For each one of the molding processes, ten parts were molded with the same set of process
29 parameters and then characterized. In order to achieve adequate stability for both molding processes, 20
30 molding cycles were performed before the collection of the first part. Then, for each molding technology,
31 the parts for the characterization were collected, one every 5 cycles.
32
33
34
35

36 **2.6 Characterization of the molded parts**

37 **2.6.1 Mechanical properties**

38 The mechanical behavior of the molded micro parts was characterized by means of uniaxial tensile
39 tests at room temperature using a mechanical testing system (Biomomentum, Mach-1TM), equipped with
40 a 25 N load cell. The molded samples were fixed using custom grips and the tests were performed with
41 a tensile speed of 10 mm/min. Elastic modulus, stress at break and strain at break were taken into
42
43
44
45
46
47
48
49
50
51
52
53
54
55
56
57
58
59
60
61
62
63
64
65

1
2
3
4 consideration for the comparison of the mechanical properties of the samples molded with the two
5
6 different injection molding technologies.
7
8
9

10 11 **2.6.2 Evaluation of crystallinity** 12 13

14 The use of ultrasound to melt the polymer and the consequent filling mechanism can affect the
15
16 formation of crystalline structure within the solidifying polymer [30]. Thus, the flow-induced
17
18 crystallization of the molded micro parts was evaluated by means of Differential Scanning Calorimetry
19
20 (DSC - TA Instruments, Discovery).
21
22

23 Thermal analysis were conducted on samples that were cut from the gauge section of the molded
24
25 micro tensile specimens. Thermal cycles were conducted with a rate of 10°C/min and by following a
26
27 heating/cooling/heating procedure, as shown in Fig. 4. Indeed, the molded polymer samples initially
28
29 present the morphological structure as induced by the processing conditions. Upon the first heating ramp,
30
31 the sample is melted and in the next cooling and heating cycles it crystallizes at much lower heating rates,
32
33 resulting in higher crystallinity. The crystallinity induced by injection molding processing was evaluated
34
35 as the ratio between the enthalpy of the first and second heating cycles.
36
37
38
39
40
41
42
43
44
45
46
47
48
49
50
51
52
53
54
55
56
57
58
59
60
61
62
63
64
65

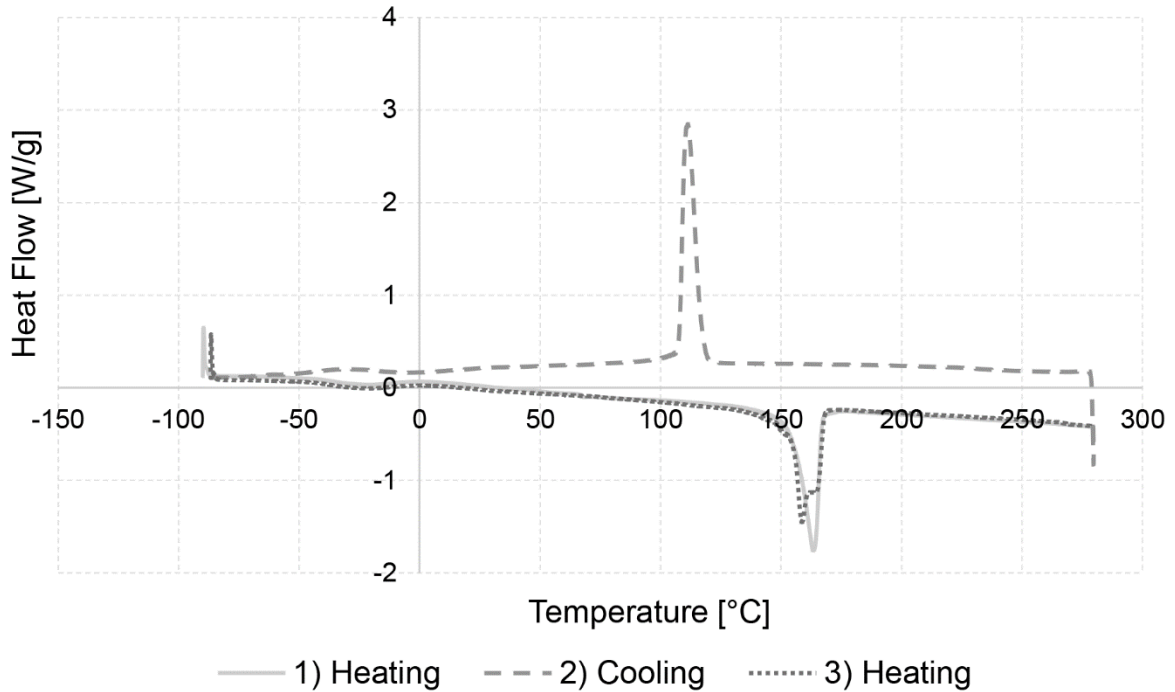


Figure 4. Procedure adopted for the DSC thermal characterization of the injection molded samples.

2.6.3 Morphological characterization

The effect of injection molding processing on the morphology of the polymer parts was characterized using a modular small- (SAXS) and wide-angle (WAXS) x-ray scattering system (Anton-Paar, SAXSpace system). An additional hot-pressed PP sample was prepared to compare the scattering results from usIM and μ IM experiments to those from a zero shear process.

An x-ray radiation with a wavelength 0.154 nm was generated at 50 kV and 1 mA. Sample-to-detector distances of 112 mm and 308 mm were used for WAXS and SAXS measurements, respectively. Debye diffractions were recorded across the whole thickness, twice at each position. Samples were rotated to obtain a full 90° diffraction of the sample to overcome detector limitation and the beam was fixed in the transverse direction (TD) perpendicular to the flow direction (MD). Scattering data were processed using Anton-Paar's SAXSTreat software.

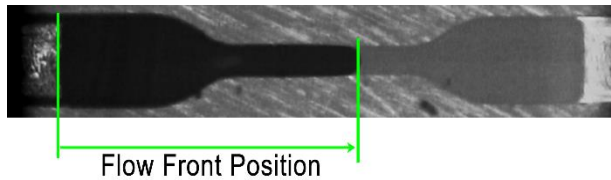
1
2
3
4
5
6
7 **3. Flow visualization setup**

8
9 **3.1 High-speed imaging**

10
11 The filling behavior in the usIM process was compared to that of the μ IM process by direct high-
12 speed imaging of the melt flow. The position of the advancing melt flow front was observed during the
13 processes using a NAC, Memrecam HX-6 camera and a compact telecentric lens (Edmund Optics,
14 Techspec[®]) with a magnification 0.75x and a working distance of 110 mm. The polymer flow was
15 illuminated using a white light LED illuminator (SugarCUBE[™], LED Illuminator) connected to a fiber
16 optic light guide.
17
18
19
20
21
22
23
24

25
26 Frame rates of 20,000 fps and 5,000 fps were adopted for the μ IM and usIM experiments,
27 respectively. The frame size (i.e. field of view) was of 640x128 pixels and the resolution of 70 pixels/mm.
28 For both processes, the recording was triggered using a digital signal output from the machine that was
29 synchronous with the initial forward movement of the injection plunger during injection, after the mold
30 closed to the viewing position.
31
32
33
34
35
36 closed to the viewing position.
37

38 The acquired image sequences were analyzed using Labview 2013[®] (National Instruments).
39 Specifically, the ‘Edge detector’ function, implemented in a National Instruments Vision Assistant
40 subVI, was used to automatically determine the coordinates of the flow front position for each one of the
41 acquired frames, as indicated in Fig. 5.
42
43
44
45
46
47



58 Figure 5. Edge detection of the flow front position on the acquired frame.
59
60
61
62
63
64
65

3.2 Thermal imaging

The temperature distribution during the filling phase was evaluated using thermal imaging of the melt flow. The thermal analysis of the cavity filling was performed using a high-speed, high-sensitivity infrared camera (FLIR, X6540SC). The camera has 640x512 pixels focal plane array (FPA) detector, operates in the spectral range of 1.5-5.1 μm , has pixel pitch of 15 μm and aperture of f/3. Detector sensitivity at 25 °C (NETD) is smaller than 20 mK.

For the usIM experiments frame size of 640x104 pixels (9.60x1.56 mm), integration time of 50 μs and frame rate of 500 fps were used. A higher frame rate was adopted for the μIM process, due to the faster melt flow velocity. For this reason, the frame size was reduced to 640x8 pixels (through the middle of the cavity) allowing to capture thermal data at the frame rate of 2,500 fps. The integration time was kept unchanged at 50 μs .

Polymer melts emit thermal radiation energy from their core, both on their surface and subsurface. Thus, radiation characteristics not only depend on cavity geometry (i.e. mainly thickness) but also on melt flow temperature distribution. This makes the polymer semi-transparent in near to mid infrared regions and interpretation of thermo-camera measurements complicated. In this work, the measurement of polymer surface temperature was carried out by compounding the base polypropylene with 4% (weight) of carbon black (CB) pigment [31], which makes it opaque in the infrared region where the thermo-camera has the highest sensitivity (i.e. 3-5 μm). Conversely, temperature measurements of unfilled polypropylene (PP) during injection molding processing were considered as volumetric/bulk values. Then, the effect of ultrasound melting on temperature distribution in the melt flow were compared to conventional μIM by setting emissivity to 1 for both unfilled and CB filled PP.

4. Results of molded parts characterization

4.1 Mechanical properties

The mechanical properties of the molded micro tensile specimens were characterized and the effect of ultrasound melting was evaluated by comparison with parts molded by conventional μ IM. Fig. 6 shows the results of the tensile strength tests, indicating that the overall mechanical properties achieved with the usIM process are higher than those obtained by μ IM. Specifically, the parts molded using the usIM machine are characterized on average by a higher value of the maximum tensile strength (+10%) compared to the μ IM samples. Similarly, the average value of the strain at break was higher (+12%) for the samples produced by usIM. The values of the elastic modulus were of similar magnitude comparing the two injection molding technologies.

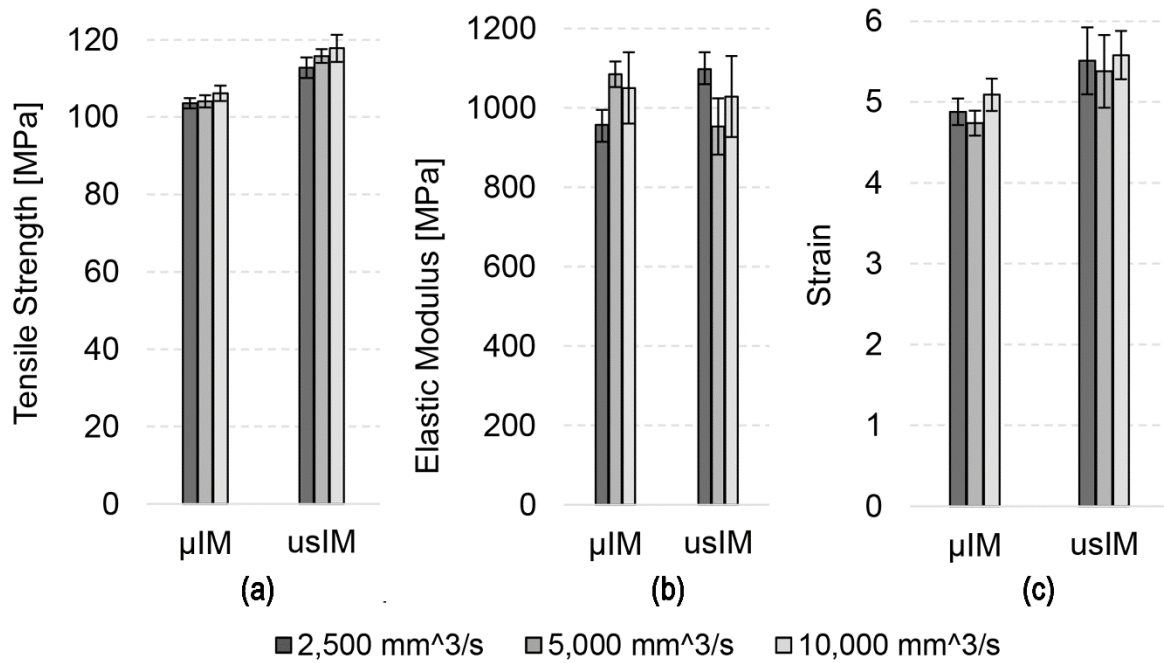


Figure 6. Mechanical properties of the micro parts molded with the two processes.

All the evaluated tensile parameters resulted more dispersed for the parts molded with the usIM than those produced by μ IM, indicating lower consistency of their mechanical properties. Moreover, no significant effect of the injection speed was observed for both μ IM and usIM.

1
2
3
4
5
6
7
8
9
10
11
12
13
14
15
16
17
18
19
20
21
22
23
24
25
26
27
28
29
30
31
32
33
34
35
36
37
38
39
40
41
42
43
44
45
46
47
48
49
50
51
52
53
54
55
56
57
58
59
60
61
62
63
64
65

Fig. 7 shows mass values of molded parts, indicating higher dispersion for usIM parts that led to higher variability of the mechanical properties. This is explained by the lower repeatability and consistency of ultrasound melting in comparison to conventional melting carried out with a reciprocating screw. In general, melting and filling behavior in usIM clearly affect the mechanical properties of the micro parts, thus indicating the need for further clarification about the melting and filling mechanisms.

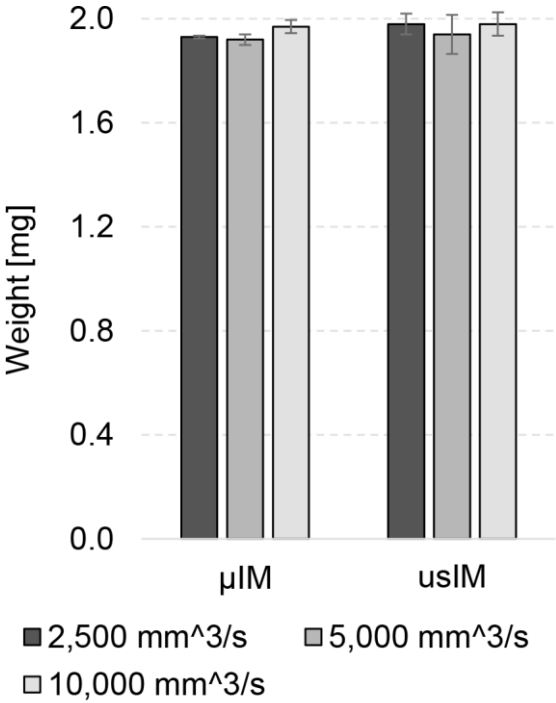


Figure 7. Weight of the micro parts molded with both processes.

4.2 Crystallinity of the molded parts

Table 2 reports the results of the DSC characterization performed on parts molded with the two different molding technologies. The results suggest higher crystallization in the usIM parts that are characterized by higher melting enthalpy. In fact, the ratio between the melting enthalpy, measured

1
2
3
4 during the first and second heating ramp, is higher for parts molded using the ultrasound melting
5
6 technology.

7
8
9 The higher level of crystallinity in the usIM samples supports the results of the mechanical
10
11 characterization. Indeed, the alignment of macromolecular chains in the crystalline structure increases
12
13 the mechanical properties of the polymer and thus the tensile resistance of the usIM molded samples
14
15 [32].
16
17
18
19
20

21 Table 2. Results of DSC characterization of the molded micro parts.
22

	Injection Speed [mm/s]	Melting 1		Melting 2		Melting1/Melting2
		Mean Val.	Std. Dev.	Mean Val.	Std. Dev.	
μIM	128	77	2	89	3	0,87
	256	79	1	90	2	0,88
	512	81	4	91	3	0,89
usIM	50	90	3	92	3	0,98
	100	86	4	89	2	0,97
	200	88	2	91	1	0,97

4.3 Flow-induced crystallization

40
41
42 The morphology of the crystalline structured yielded by the different injection molding technologies
43
44 was analyzed by overlaying WAXS 2D images for diffraction angles between 0 and 90°. Samples molded
45
46 using usIM are characterized, for all values of the injection speed, by isotropic scattering due to the
47
48 formation of spherulites, as shown in Fig. 8 (b). Similar scattering behavior was observed for the hot
49
50 pressed samples (Fig. 8 (a)), which were obtained under zero-shear conditions. Conversely, μIM samples
51
52 exhibit anisotropic scattering (Fig. 8 (c), (d), (e)) with dominant reflections at plane positions (110), (040)
53
54 and (130), which are typical of α-crystalline phase. Additional diffraction at position (300) indicates the
55
56 formation of β-phase.
57
58
59
60
61
62
63
64
65

1
2
3
4
5
6
7
8
9
10
11
12
13
14
15
16
17
18
19
20
21
22
23
24
25
26
27
28
29
30
31
32
33
34
35
36
37
38
39
40
41
42
43
44
45
46
47
48
49
50
51
52
53
54
55
56
57
58
59
60
61
62
63
64
65

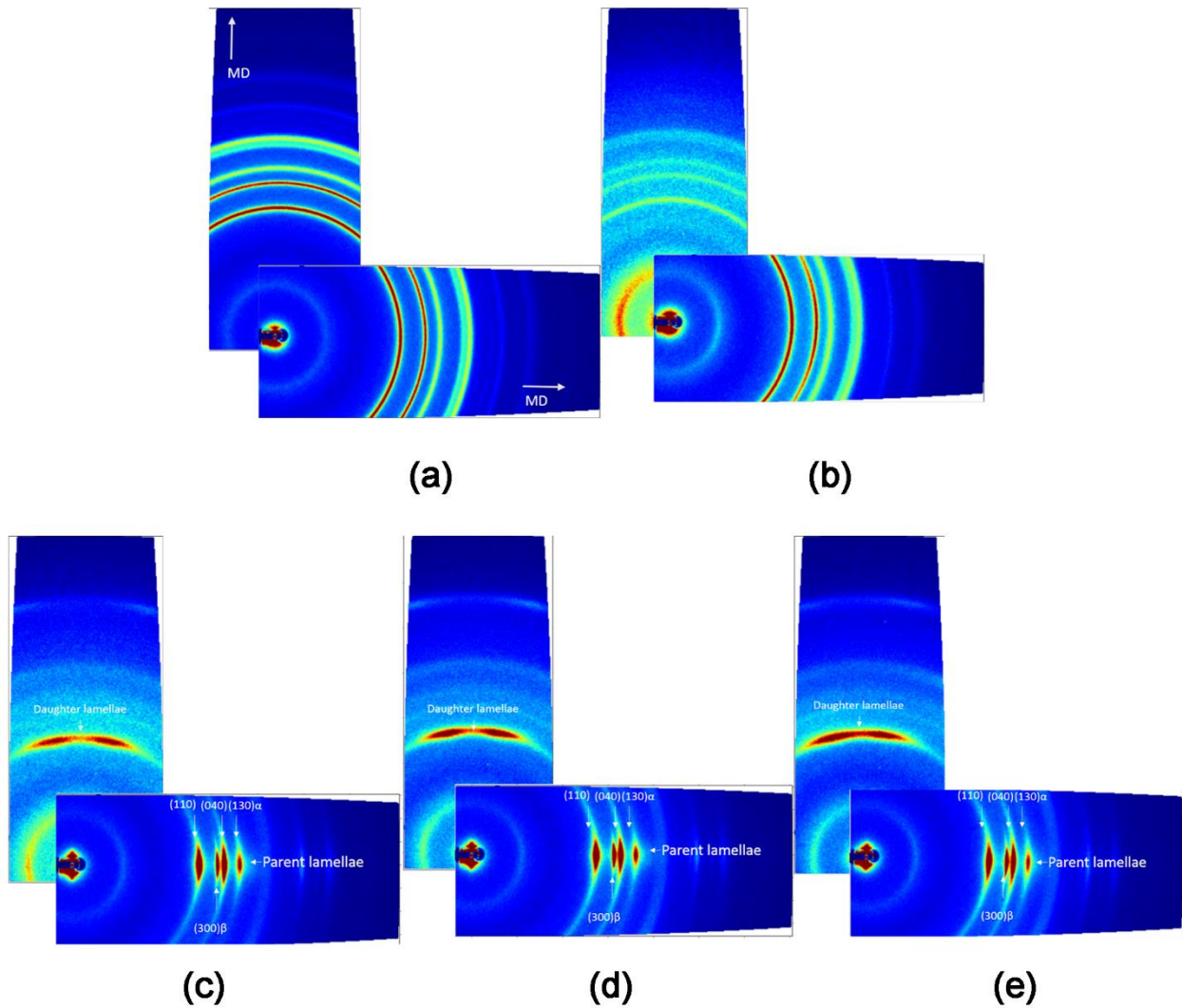


Figure 8. WAXS scattering patterns for a) hot pressed PP, b) usIM, c) μ IM at 2,500 mm^3/s d) μ IM at 5,000 mm^3/s and e) μ IM at 10,000 mm^3/s .

Giving a broad azimuthal distribution to plane (110), scattering diffraction in an equatorial direction represents ‘parent lamellae’, which are crystals growing in the flow direction (c - axis) [30]. Double intensity spots in the meridional direction represent the ‘daughter lamellae’, which are formed by ‘lamellar branching’ propagation of the crystal epitaxial growth along the a^* - axis (i.e. perpendicular to

the c - axis). The growth in both directions was evaluated considering the relative intensity of reflections in the (110) plane and by applying the Fujiyama method [33]:

$$[a^*]_{110} = \frac{a^*}{c+a^*} \quad (1)$$

where C is the area around the azimuthal angle of 0° and a^* the area around 90° , as shown in Fig. 9.

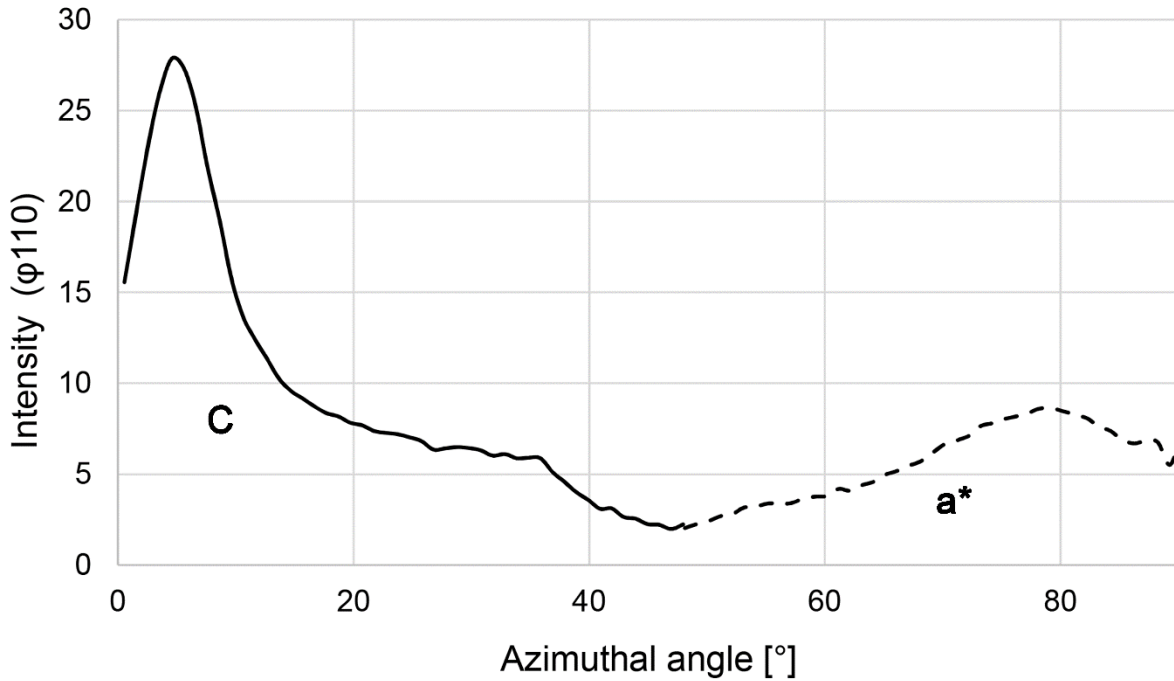


Figure 9. Fujiyama method to determine lamellar branched structure.

Table 3 reports the results of the morphological characterization for the molded micro parts. The fraction a^* was found to be zero for the hot-pressed sample and 0.01 for the usIM samples, indicating the absence of ‘lamellar branching’. Marked growth of crystals (i.e. high values of a^*) was observed in the μ IM samples where higher shear rates characterize the filling of the cavity.

Table 3. Relative a^* orientation values calculated for the different samples.

Sample	$[a^*]_{110}$
--------	---------------

hot-pressed	0.00
usIM	0.01
μ IM 2,500 mm ³ /s	0.24
μ IM 5,000 mm ³ /s	0.35
μ IM 10,000 mm ³ /s	0.48

Fig. 10 shows SAXS images obtained from the characterization of the different samples. Isotropic scattering in hot-pressed and usIM samples confirm the absence of flow-induced orientation in these samples. Moreover, for the usIM parts no significant effect of higher injection speed was observed. SAXS analysis of μ IM parts confirmed scattering diffraction at plane (110) due to the formation of α -crystalline phase and meridional high intensity tear drop spots (kebab structure), which originates from the lamellae in the flow direction (shish).

In general, the results of the morphological characterization provide evidence of different filling mechanisms in the usIM and μ IM processes. In particular, the comparison of usIM samples with those obtained by hot pressing confirms the very low shear rates during filling. Conversely, higher flow-induced crystallization and higher orientation of the crystal characterize parts obtained by μ IM, and this effect is increasingly evident for higher μ IM injection speed. When using ultrasound melting, the effect of higher injection speed values is not significant, indicating a possible interaction between the melting and filling phases in the usIM process [34].

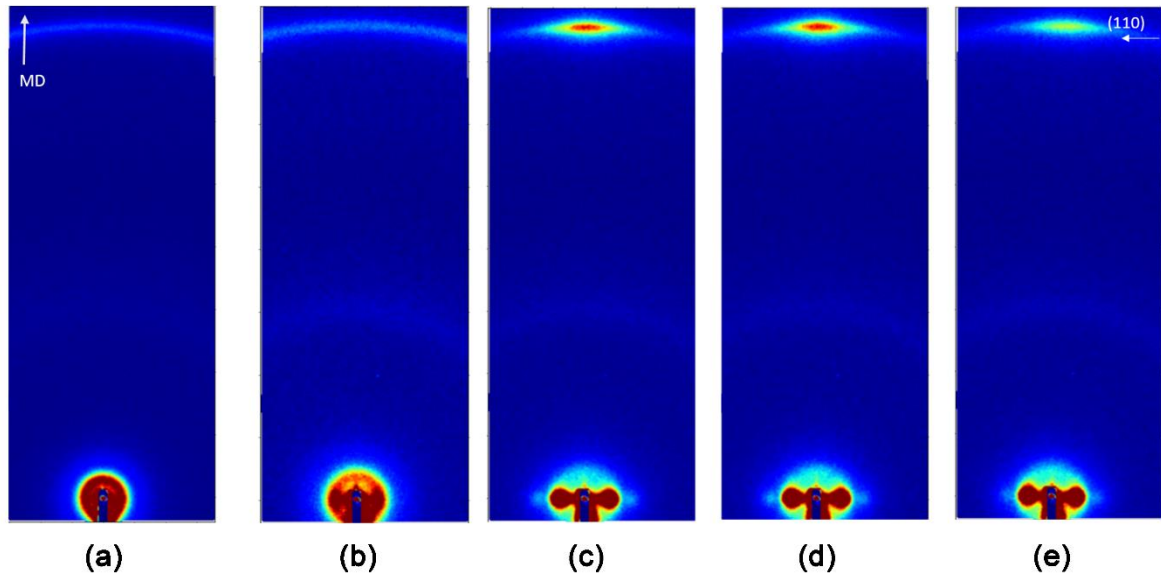


Figure 10. SAXS results of the tested samples for a) hot pressed PP, b) usIM, c) μ IM at 2,500 mm^3/s , d) μ IM at 5,000 mm^3/s and e) μ IM 10,000 at mm^3/s . MD (flow direction) is vertical.

5. Results of flow visualization

5.1 Cavity filling times

The effect of ultrasound melting on the speed of the injected polymer melt was evaluated by tracking the coordinates of the advancing flow front from the moment it entered the cavity until it reached its far end. Then, knowing the value of the frame rate used for the acquisition it was possible to link the specific position to its specific time.

Figure 11 reports the results of the flow visualization analysis, showing different trends for the flow front position during cavity filling in the two molding technologies. For the μ IM process (Fig. 11 (a)), the filling of the tensile bar cavity is characterized by changes of the speed (i.e. slope of the curve) in the three main sections (gate tab, gauge length and end tab). Conversely, for the usIM process no clear distinction is observed between the speed of the polymer in the gauge length and in the end tab (Fig. 11 (b)).

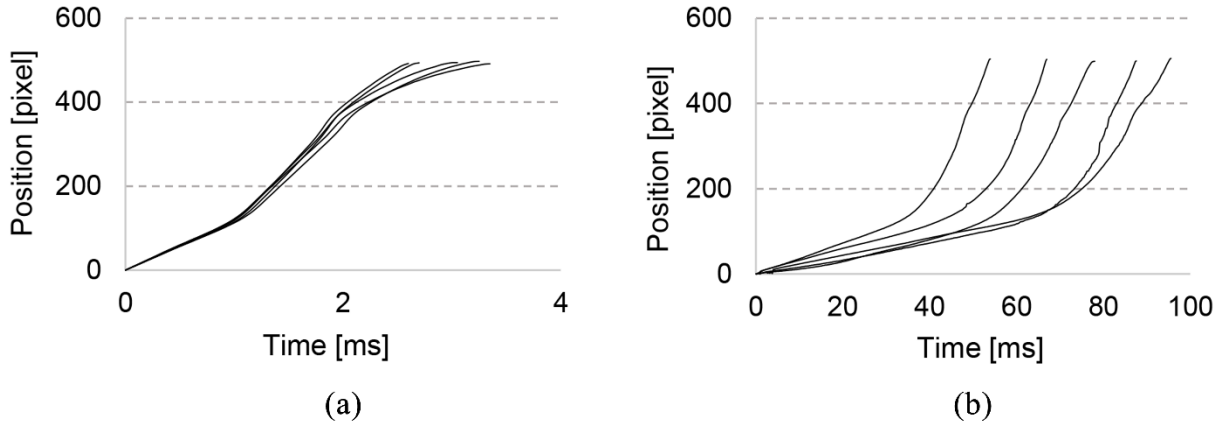


Figure 11. Flow front tracking for five repeated (a) micro injection molding and (b)

ultrasound injection molding experiments for a set flow rate of $5000 \text{ mm}^3/\text{s}$. The curves in both plots represent repetitions of experiments performed with the same set of process parameters with the two processes.

The results of the flow front position tracking analysis allowed the evaluation of the filling time for both processes and for the selected values of the injection speed. The times required to fill the cavity are significantly higher for the usIM process compared to μIM (Table 4). Moreover, the values of the filling time calculated are more dispersed, indicating smaller consistency of cavity filling when using ultrasound melting.

Table 4. Filling times obtained from the high-speed camera acquisitions for the processes.

Process	Injection Speed [mm/s]	Filling Time [ms]	
		Avg. Val.	Std. Dev.
Micro Injection Molding	128	3.4	0.1
	256	3.0	0.3
	512	1.6	0.2
Ultrasound Injection Molding	50	57.5	9.6
	100	76.0	16.0
	200	70.0	12.0

5.2 Effect of the injection speed

The filling behavior of the melt polymer in the two processes was also investigated as a function of the injection speed. The effect of higher flow rate resulted in a decrease of the filling time in the μ IM process, while no significant variations were observed for the usIM process (Fig. 12). In fact, in the μ IM process, the injection plunger exerts its action on a defined amount of polymer, which was previously melted by the mechanical action of a reciprocating screw and then maintained in isothermal conditions. Conversely, in the usIM process, the ultrasonic vibration progressively melts the polymer while the injection plunger moves upwards pushing the material to promote the injection of the molten polymer into the cavity. In these conditions, the injection plunger is acting on a polymer characterized by inhomogeneous thermal and rheological properties. Hence, in the usIM process, the melting and filling phases are simultaneous and they interact. Consequently, the filling time for the usIM process is mainly controlled by the melting rate, which depends on the ultrasound vibration characteristics.

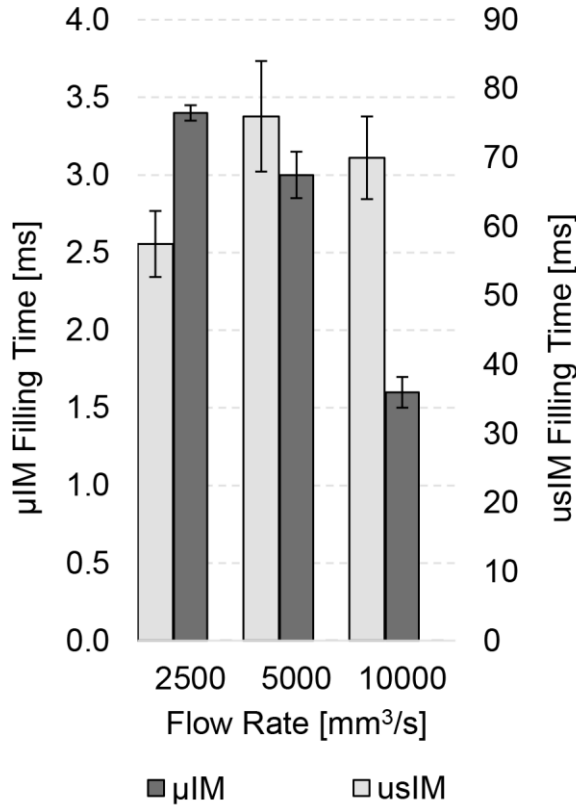


Figure 12. Cavity filling times for both processes as a function of the different set flow rates.

The high-speed camera acquisitions were also used to determine the actual values of the flow front speed during filling of the cavity. The acquired image sequences were processed using NI Vision Assistant only in the gauge section of the cavity, which is characterized by a rectangular cross section (250x400 μm). The flow front speed of the injected polymer was determined as the gradient of the advancing flow front position over time and the actual volumetric flow rate was then calculated.

Table 5 reports the calculated flow front speed for the polymer flowing in the gauge length section of the cavity for both processes. The results indicate that the tracked speed of the polymer melt in the cavity is markedly higher for the μIM process compared to the usIM. Moreover, for the latter the effect of changing the injection speed was confirmed to be negligible.

Table 5. Results of edge detection analysis for the processes and different values of the injection speed.

Process	Set Flow Rate	Flow Front Speed [mm/s]	
	[mm ³ /s]	Avg. Val.	Std. Dev.
Micro Injection Molding	2500	2970	180
	5000	3834	185
	10000	7346	705
Ultrasound Injection Molding	2500	259	35
	5000	226	33
	10000	219	17

5.3 Melt flow temperature

The temperature of the polymer melt flow during the molding cycle was characterized by means of high-speed thermal imaging, as shown in Fig. 13. Profiles acquired during the μ IM cycle are characterized by a steep growth of the temperature during the filling phase and the maximum temperature was acquired at the flow front. Moreover, temperature acquisitions for μ IM are characterized by high consistency for acquisitions repeated at constant value of the injection speed.

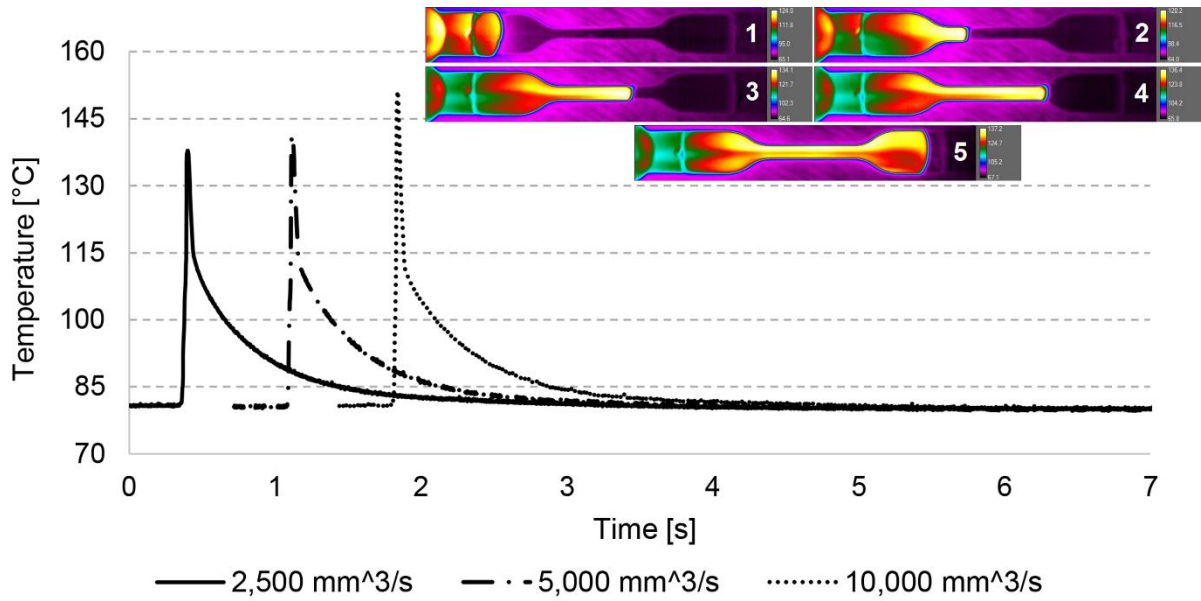


Figure 13. Repeated acquisitions of temperature profiles during μ IM cycles at different values of the injection speed.

Conversely, several temperature peaks were observed during the usIM cycle due the different melting and injection mechanisms (Fig. 14 (a)). Indeed, while the ultrasound vibration is maintained (i.e. for 2 seconds), the polymer is progressively melted and injected into the cavity, thus resulting in a temperature distribution within the melt flow that is different from that of conventional μ IM. Specifically, heat convection from the melt polymer flowing to the cavity lead to higher temperature close to the injection location. Hence, heat is continuously convected through the gate and the polymer is progressively colder moving towards the flow front.

Fig. 14 (b) reports the temperature, the ultrasonic power and the force curves monitored for a single usIM cycle, comparing them with thermal frames. A correlation between the ultrasonic power and the temperature of the polymer melt during filling in the usIM was observed. Specifically, the first material reaches the injection location (frame #1) just after the first peak of in the ultrasound power profile. The filling of the cavity is accompanied by repeated peaks of both temperature and power, as shown in frames

#2, #3 and #4. Since, the vibration and the force are maintained after the achievement of the complete filling of the mold cavity, further material flows into the cavity and packing occurs (cf. frame #5 and #6).

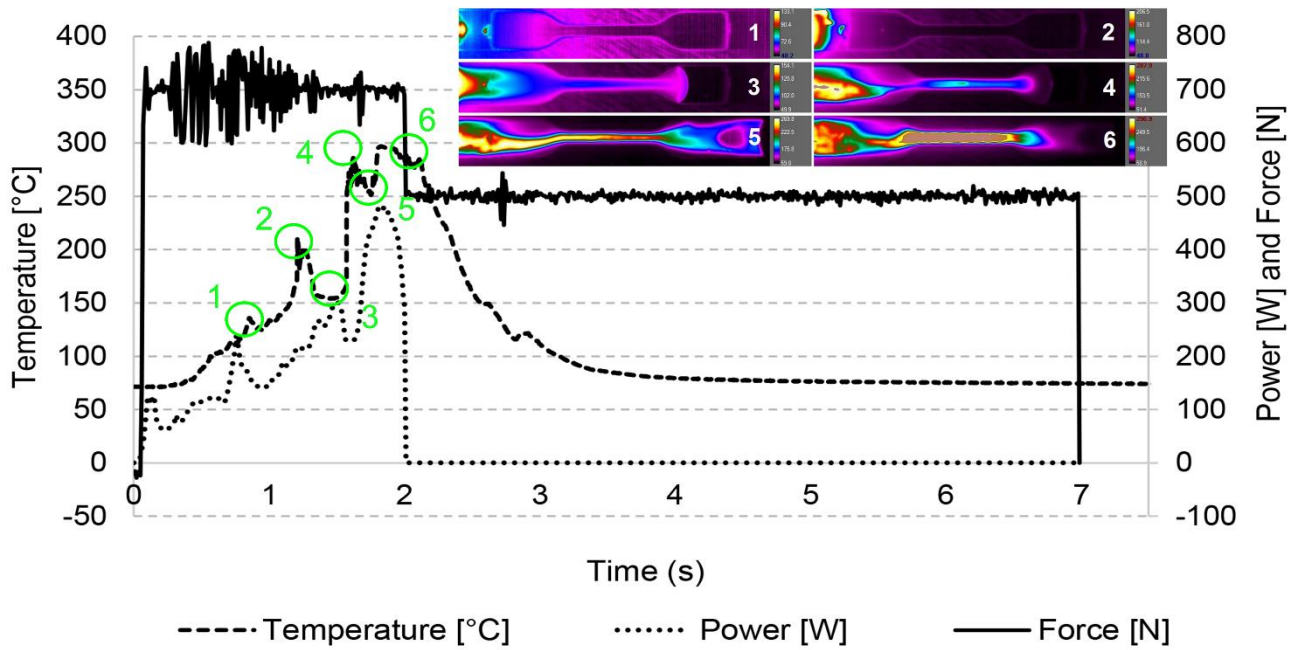
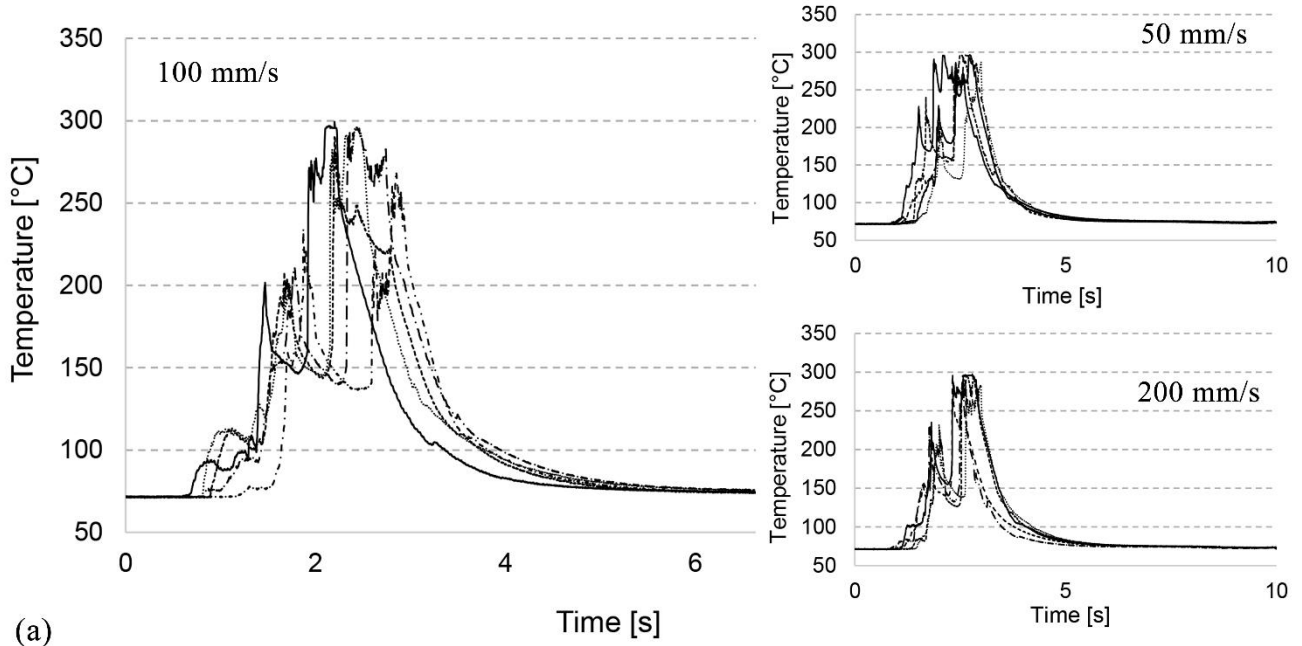


Figure 14. (a) Repeated acquisitions of temperature profiles during μ IM cycles at different values of the injection speed and (b) comparison of temperature, power and force profiles.

Higher values of the injection speed resulted in higher temperature for the μ IM process, while no significant variation was observed for the usIM process. Indeed, in the usIM process, the filling of the cavity is controlled by the melting rate, as discussed in Section 5.2.

Fig. 15 reports the maximum values of temperature acquired within the polymer during injection for the two different molding technologies. When using ultrasound vibration to melt the plastic granules, markedly higher temperature peaks were observed. In fact, the heat convected during the progressive melting and injection lead to higher temperature of the polymer melt. Conversely, in μ IM the heat convected by the advancing flow front is rapidly dissipated by conduction through the mold surface.

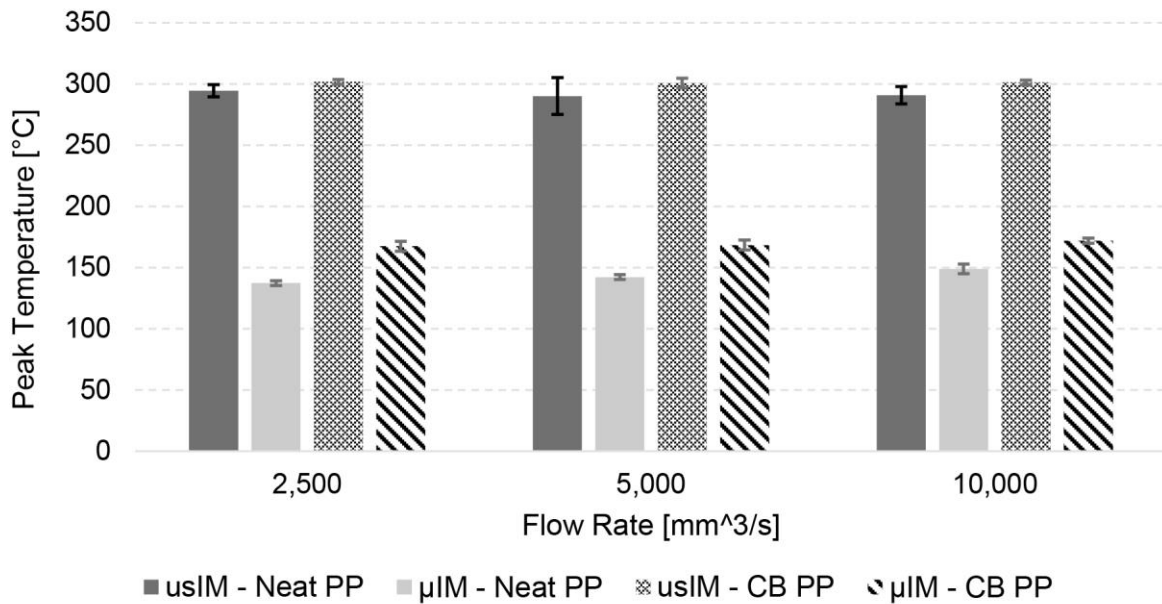


Figure 15. Peak temperatures for the usIM and μ IM processes.

6. Conclusion

1
2
3
4
5
6
7
8
9
10
11
12
13
14
15
16
17
18
19
20
21
22
23
24
25
26
27
28
29
30
31
32
33
34
35
36
37
38
39
40
41
42
43
44
45
46
47
48
49
50
51
52
53
54
55
56
57
58
59
60
61
62
63
64
65

In this work, the ultrasound injection molding process was experimentally compared to the conventional micro injection molding process. The molding of micro tensile bars allowed the characterization of the effect of ultrasound melting on the mechanical properties of polypropylene micro parts. A comprehensive characterization of the filling behavior of the two processes was carried out by means of high-speed thermal and conventional direct flow visualization.

The tensile properties of the molded micro parts indicated that the overall mechanical properties achieved with the usIM process are not just comparable to those obtained with the μ IM, but offer significantly improved performance. However, the smaller repeatability in the mechanical behavior of the parts molded with usIM are due to the higher weight variability.

The results of the tracking of the flow front positions showed that μ IM is characterized by a more consistent and repeatable filling behavior compared to usIM. In particular, in the conventional process increasing the injection speed resulted in significantly higher flow front speed, while the usIM had no significant effect on increasing the flow rate. This different response to the change of the set flow rate can be reconducted to the different melting mechanisms. In fact, compared to the conventional melting, which is carried out with a reciprocating screw, the use of ultrasound vibration leads to inhomogeneous thermal and rheological conditions of the polymer melt.

Moreover, the ultrasound melting resulted in higher temperature of the injected polymer melt due to the sustainment of the ultrasound vibration during filling and packing phases. Indeed, several temperature peaks were observed close to the injection location and not on the flow front as in the conventional μ IM process.

1
2
3
4
5
6
7
8
9
10
11
12
13
14
15
16
17
18
19
20
21
22
23
24
25
26
27
28
29
30
31
32
33
34
35
36
37
38
39
40
41
42
43
44
45
46
47
48
49
50
51
52
53
54
55
56
57
58
59
60
61
62
63
64
65

Funding

This research did not receive any specific grant from funding agencies in the public, commercial, or not-for-profit sectors.

References

- [1] Attia, U. M., Marson, S., & Alcock, J. R. (2009). Micro-injection moulding of polymer microfluidic devices. *Microfluidics and Nanofluidics*, 7(1), 1-28.
- [2] Tseng, S. C., Chen, Y. C., Kuo, C. L., & Shew, B. Y. (2005). A study of integration of LIGA and M-EDM technology on the microinjection molding of ink-jet printers' nozzle plates. *Microsystem technologies*, 12(1-2), 116-119.
- [3] Angelov, A. K., & Coulter, J. P. (2008). The development and characterization of polymer microinjection molded gratings. *Polymer Engineering & Science*, 48(11), 2169-2177.
- [4] Wallrabe, U., Dittrich, H., Friedsam, G., Hanemann, T., Mohr, J., Müller, K., ... & Zißler, W. (2002). Micromolded easy-assembly multi fiber connector: RibCon®. *Microsystem technologies*, 8(2-3), 83-87.
- [5] Lucchetta, G., Sorgato, M., Zanchetta, E., Brusatin, G., Guidi, E., Di Liddo, R., & Conconi, M. T. (2015). Effect of injection molded micro-structured polystyrene surfaces on proliferation of mc3t3-e1 cells. *Express Polym Lett*, 9(4), 354-361.
- [6] Masato, D., Sorgato, M., Babenko, M., Whiteside, B., & Lucchetta, G. (2017). Thin-wall injection molding of polystyrene parts with coated and uncoated cavities. *Materials & Design*, 141, 286-295.
- [7] Masato, D., Sorgato, M., Parenti, P., Annoni, M., & Lucchetta, G. (2017). Impact of deep cores surface topography generated by micro milling on the demolding force in micro injection molding. *Journal of Materials Processing Technology*, 246, 211-223.
- [8] Yang, C., Yin, X. H., & Cheng, G. M. (2013). Microinjection molding of microsystem components: new aspects in improving performance. *Journal of Micromechanics and Microengineering*, 23(9), 093001.

- 1
2
3
4 [9] Whiteside, B. R., Martyn, M. T., Coates, P. D., Allan, P. S., Hornsby, P. R., & Greenway, G.
5
6 (2003). Micromoulding: process characteristics and product properties. *Plastics, rubber and composites*,
7
8 32(6), 231-239.
9
- 10 [10] Hansen, H. N., Hocken, R. J., & Tosello, G. (2011). Replication of micro and nano surface
11
12 geometries. *CIRP Annals-Manufacturing Technology*, 60(2), 695-714.
13
- 14 [11] Sorgato, M., Masato, D., & Lucchetta, G. (2016). Effect of vacuum venting and mold
15
16 wettability on the replication of micro-structured surfaces. *Microsystem Technologies*, 1-10.
17
18
- 19 [12] Masato, D., Sorgato, M., & Lucchetta, G. (2016). Analysis of the influence of part thickness on
20
21 the replication of micro-structured surfaces by injection molding. *Materials & Design*, 95, 219-224.
22
23
- 24 [13] Sorgato, M., Babenko, M., Lucchetta, G., & Whiteside, B. (2017). Investigation of the influence of
25
26 vacuum venting on mould surface temperature in micro injection moulding. *The International Journal*
27
28 *of Advanced Manufacturing Technology*, 88(1-4), 547-555.
29
30
- 31 [14] Lucchetta, G., Sorgato, M., Carmignato, S., & Savio, E. (2014). Investigating the technological
32
33 limits of micro-injection molding in replicating high aspect ratio micro-structured surfaces. *CIRP*
34
35 *Annals-Manufacturing Technology*, 63(1), 521-524.
36
37
- 38 [15] Masato, D., Rathore, J., Sorgato, M., Carmignato, S., & Lucchetta, G. (2017). Analysis of the
39
40 shrinkage of injection-molded fiber-reinforced thin-wall parts. *Materials & Design*, 132, 496-504.
41
42
- 43 [16] Lucchetta, G., Masato, D., Sorgato, M., Crema, L., & Savio, E. (2016). Effects of different
44
45 mould coatings on polymer filling flow in thin-wall injection moulding. *CIRP Annals-Manufacturing*
46
47 *Technology*, 65(1), 537-540.
48
49
- 50 [17] Giboz, J., Copponnex, T., & Mélé, P. (2009). Microinjection molding of thermoplastic
51
52 polymers: morphological comparison with conventional injection molding. *Journal of Micromechanics*
53
54 *and Microengineering*, 19(2), 025023.
55
56
57
58
59
60
61
62
63
64
65

- 1
2
3
4 [18] Michaeli, W., Spennemann, A., & Gärtner, R. (2002). New plastification concepts for micro
5 injection moulding. *Microsystem technologies*, 8(1), 55-57.
6
7
8
9 [19] Michaeli, W., Kamps, T., & Hopmann, C. (2011). Manufacturing of polymer micro parts by
10 ultrasonic plasticization and direct injection. *Microsystem Technologies*, 17(2), 243-249.
11
12
13
14 [20] Wu, W., Peng, H., Jia, Y., & Jiang, B. (2016). Characteristics and mechanisms of polymer
15 interfacial friction heating in ultrasonic plasticization for micro injection molding. *Microsystem*
16 *Technologies*, 1-8.
17
18
19 [21] Jiang, B., Peng, H., Wu, W., Jia, Y., & Zhang, Y. (2016). Numerical Simulation and
20 Experimental Investigation of the Viscoelastic Heating Mechanism in Ultrasonic Plasticizing of
21 Amorphous Polymers for Micro Injection Molding. *Polymers*, 8(5), 199.
22
23
24 [22] Chen, G., Guo, S., & Li, H. (2002). Ultrasonic improvement of rheological behavior of
25 polystyrene. *Journal of applied polymer science*, 84(13), 2451-2460.
26
27
28 [23] Chen, J., Chen, Y., Li, H., Lai, S. Y., & Jow, J. (2010). Physical and chemical effects of
29 ultrasound vibration on polymer melt in extrusion. *Ultrasonics sonochemistry*, 17(1), 66-71.
30
31
32 [24] Ávila- Orta, C., Espinoza- González, C., Martínez- Colunga, G., Bueno- Baqués, D.,
33 Maffezzoli, A., & Lionetto, F. (2013). An overview of progress and current challenges in ultrasonic
34 treatment of polymer melts. *Advances in Polymer Technology*, 32(S1), E582-E602.
35
36
37 [25] Sacristan, M., Planta, X., Morell, M., & Puiggali, J. (2014). Effects of ultrasonic vibration on
38 the micro-molding processing of polylactide. *Ultrasonics sonochemistry*, 21(1), 376-386.
39
40
41 [26] Grabalosa, J., Ferrer, I., Elías-Zúñiga, A., & Ciurana, J. (2016). Influence of processing
42 conditions on manufacturing polyamide parts by ultrasonic molding. *Materials & Design*, 98, 20-30.
43
44
45 [27] Michaeli, W., & Starke, C. (2005). Ultrasonic investigations of the thermoplastics injection
46 moulding process. *Polymer testing*, 24(2), 205-209.
47
48
49
50
51
52
53
54
55
56
57
58
59
60
61
62
63
64
65

- 1
2
3
4 [28] Negre Gubau, P., Grabalosa Saubí, J., Ferrer Real, I., & Ciurana, Q. D. (2015). Study of the
5 ultrasonic molding process parameters for manufacturing polypropylene parts. *Procedia Engineering*,
6 2015, vol. 32, p. 7-14.
7
8
9
10 [29] Whiteside, B. R., Spares, R., Brown, E. C., Norris, K., Coates, P. D., Kobayashi, M., ... &
11 Cheng, C. C. (2008). Optical imaging metrology for micromoulding cavity flows and products.
12 *Plastics, Rubber and Composites*, 37(2-4), 57-66.
13
14 [30] Ma, Z., Balzano, L., Portale, G., & Peters, G. W. (2014). Flow induced crystallization in
15 isotactic polypropylene during and after flow. *Polymer*, 55(23), 6140-6151.
16
17 [31] Babenko, M., Sweeney, J., Petkov, P., Lacan, F., Bigot, S., & Whiteside, B. (2017). Evaluation
18 of Heat Transfer at the Cavity-Polymer Interface in Microinjection Moulding based on Experimental
19 and Simulation Study. *Applied Thermal Engineering*.
20
21 [32] Fischer, C., & Drummer, D. (2016). Crystallization and mechanical properties of polypropylene
22 under processing-relevant cooling conditions with respect to isothermal holding time. *International
23 Journal of Polymer Science*, 2016.
24
25 [33] Schrauwen, B. A., Janssen, R. P., Govaert, L. E., & Meijer, H. E. (2004). Intrinsic deformation
26 behavior of semicrystalline polymers. *Macromolecules*, 37(16), 6069-6078.
27
28 [34] Gao, S., Qiu, Z., Ma, Z., & Yang, Y. (2017). Flow properties of polymer melt in longitudinal
29 ultrasonic- assisted microinjection molding. *Polymer Engineering & Science*, 57(8), 797-805.
30
31
32
33
34
35
36
37
38
39
40
41
42
43
44
45
46
47
48
49
50
51
52
53
54
55
56
57
58
59
60
61
62
63
64
65

1
2
3
4 **Figure captions**
5

6 *Figure 1.* Design of the molded micro part. All dimensions are in millimeters.
7

8
9 *Figure 2.* Main phases of the usIM process, (a) pellet feeding and compression, (b) melting, (c) injection.
10

11 *Figure 3.* Mold design, as mounted on the usIM machine, and indication of its main components.
12

13
14 *Figure 4.* Procedure adopted for the DSC thermal characterization of the injection molded samples.
15

16
17 *Figure 5.* Edge detection of the flow front position on the acquired frame.
18

19
20 *Figure 6.* Mechanical properties of the micro parts molded with the two processes.
21

22
23 *Figure 7.* Weight of the micro parts molded with both processes.
24

25
26 *Figure 8.* WAXS scattering patterns for a) hot pressed PP, b) usIM, c) μ IM at 2,500 mm³/s d) μ IM at 5,000
27 mm³/s and e) μ IM at 10,000 mm³/s.
28

29
30
31 *Figure 9.* Fujiyama method to determine lamellar branched structure.
32

33
34 *Figure 10.* SAXS results of the tested samples for a) hot pressed PP, b) usIM, c) μ IM at 2,500 mm³/s, d) μ IM at
35 5,000 mm³/s and e) μ IM 10,000 at mm³/s. MD (flow direction) is vertical.
36

37
38
39 *Figure 11.* Flow front tracking for five repeated (a) micro injection molding and (b) ultrasound injection molding
40 experiments for a set flow rate of 5000 mm³/s. The curves in both plots represent repetitions of experiments
41 performed with the same set of process parameters with the two processes.
42

43
44
45 *Figure 12.* Cavity filling times for both processes as a function of the different set flow rates.
46

47
48
49 *Figure 13.* Repeated acquisitions of temperature profiles during μ IM cycles at different values of the injection
50 speed.
51

52
53
54 *Figure 14.* (a) Repeated acquisitions of temperature profiles during μ IM cycles at different values of the
55 injection speed and (b) comparison of temperature, power and force profiles.
56

57
58
59 *Figure 15.* Peak temperatures for the usIM and μ IM processes.
60
61
62
63
64
65

1
2
3
4
5
6
7
8
9
10
11
12
13
14
15
16
17
18
19
20
21
22
23
24
25
26
27
28
29
30
31
32
33
34
35
36
37
38
39
40
41
42
43
44
45
46
47
48
49
50
51
52
53
54
55
56
57
58
59
60
61
62
63
64
65

Table captions

Table 1. Main properties of the polymer selected for the molding experiments.

Table 2. Results of DSC characterization of the molded micro parts.

Table 3. Relative a* orientation values calculated for the different samples.

Table 4. Filling times obtained from the high-speed camera acquisitions for the processes.

Table 5. Results of edge detection analysis for the processes and different values of the injection speed.